



PAPER

Performance evaluation of the FastIC readout ASIC with emphasis on Cherenkov emission in TOF-PET

OPEN ACCESS

RECEIVED

24 December 2023

REVISED

27 March 2024

ACCEPTED FOR PUBLICATION

24 April 2024

PUBLISHED

20 May 2024

Original content from this work may be used under the terms of the [Creative Commons Attribution 4.0 licence](#).

Any further distribution of this work must maintain attribution to the author(s) and the title of the work, journal citation and DOI.



Markus Piller^{1,2} , Antonio M Castilla³, Giulia Terragni^{1,4} , Jerome Alozy¹, Etienne Auffray¹ , Rafael Ballabriga^{1,3}, Michael Campbell¹, Bernd Deutschmann², David Gascon³ , Alberto Gola⁵ , Stefano Merzi⁵ , Alicja Michalowska-Forsyth² , Michele Penna⁵, Sergio Gómez^{3,6} and Nicolaus Kratochwil^{1,7,*}

¹ CERN, Esplanade des Particules 1, 1211 Meyrin, Switzerland

² Graz University of Technology, Institute of Electronics, A-8010 Graz, Austria

³ University of Barcelona, Spain

⁴ Technical University of Vienna, Austria

⁵ Fondazione Bruno Kessler, Via Sommarive, 18 I-38123, Trento, Italy

⁶ Serra Hunter Fellow at Polytechnic University of Catalonia, Spain

⁷ Department of Biomedical Engineering, University of California, Davis, United States of America

* Author to whom any correspondence should be addressed.

E-mail: nkratochwil@ucdavis.edu

Keywords: cherenkov emission, BGO, fastic ASIC, TOF-PET, silicon photomultiplier (SiPM), coincidence time resolution (CTR), scintillating crystal

Abstract

Objective. The efficient usage of prompt photons like Cherenkov emission is of great interest for the design of the next generation, cost-effective, and ultra-high-sensitivity time-of-flight positron emission tomography (TOF-PET) scanners. With custom, high power consuming, readout electronics and fast digitization the prospect of sub-300 ps FWHM with PET-sized BGO crystals have been shown. However, these results are not scalable to a full system consisting of thousands of detector elements. *Approach.* To pave the way toward a full TOF-PET scanner, we examine the performance of the FastIC ASIC with Cherenkov-emitting scintillators (BGO), together with one of the most recent SiPM detector developments based on metal trenching from FBK. The FastIC is a highly configurable ASIC with 8 input channels, a power consumption of 12 mW ch⁻¹ and excellent linearity on the energy measurement. To put the timing performance of the FastIC into perspective, comparison measurements with high-power consuming readout electronics are performed. *Main results.* We achieve a best CTR FWHM of 330 ps for 2 × 2 × 3 mm³ and 490 ps for 2 × 2 × 20 mm³ BGO crystals with the FastIC. In addition, using 20 mm long LSO:Ce:Ca crystals, CTR values of 129 ps FWHM have been measured with the FastIC, only slightly worse to the state-of-the-art of 95 ps obtained with discrete HF electronics. *Significance.* For the first time, the timing capability of BGO with a scalable ASIC has been evaluated. The findings underscore the potential of the FastIC ASIC in the development of cost-effective TOF-PET scanners with excellent timing characteristics.

1. Introduction

The detection chain for a light-based radiation detector system, used both in medical imaging and high energy physics experiments, comprises a scintillator to convert high energy particles into optical photons; a photodetector to convert the optical photons into an analog signal; readout electronics to amplify and/or discriminate the signal to provide information on the time-of-arrival and energy of the initial energetic particle; and lastly a data acquisition system to provide digital data for further physics analysis or image processing (Lecoq *et al* 2023).

This detector chain is complex, and to boost the performance, all components need to be optimized. For example, the state-of-the-art scintillator material for time-of-flight positron emission tomography (TOF-PET)

is based on lutetium (LSO:Ce, LYSO:Ce, LGSO:Ce and Ca/Mg co-doped variants) providing a high number of photons per energy deposition, as well as a fast scintillation response with decay times of around 40 ns (Gundacker *et al* 2016b). For better sensitivity, but also to overcome limitations based on standard scintillation, new materials and processes are investigated, such as prompt Cherenkov photon emission in BGO (Kwon *et al* 2016).

Of similar importance is the choice of the photodetector. Nowadays, silicon photomultipliers (Gundacker and Heering 2020) (SiPMs) have mostly substituted photomultiplier tubes due to their compactness, better detection efficiency, and insensitivity to magnetic fields, which can be a requirement when PET is combined with magnetic resonance imaging. Important characteristics of SiPMs for TOF-PET imaging are the photon detection efficiency (PDE), single photon time resolution (SPTR), dark count rate (DCR) and crosstalk probability (Gola *et al* 2019). On the latter, significant crosstalk reduction has been reported due to the implementation of metal-filled trenches between individual single photon avalanche diodes (SPADs) (Merzi *et al* 2023).

Major time resolution breakthroughs have been achieved by the use of custom high frequency readout electronics to mitigate the contribution of electronic noise, provide a fast output signal, and apply leading edge discrimination at the software level using the digitized waveform (Cates *et al* 2018, Gundacker *et al* 2019). However, lowering the high power consumption when using off-the-shelf electronic components (Cates *et al* 2022, Krake *et al* 2022) is mandatory in terms of scalability (Cates *et al* 2022) for a scanner, consisting of thousands of individual channels, and thus imposing a challenge that various groups are actively working on (Pourashraf *et al* 2022, Gonzalez-Montoro *et al* 2023, Lee *et al* 2023, Nadig *et al* 2023b).

Application-specific integrated circuits (ASICs) are typically applied in systems because they can process many input channels with low power consumption in a compact area. A summary of available ASICs used for TOF applications is provided in table 1. The FastIC ASIC with 8 channels is of particular interest, due to a combination of relatively low power consumption of 6–12 mW ch^{-1} depending on the operation mode, excellent linearity of the input stage (about 3% linearity error for the full energy readout), and encouraging SPTR (Gomez *et al* 2021). The latter is of the most relevance to exploit Cherenkov emission, as it is the most determining parameter to obtain a good timing capability for low light intensities (Dolenec *et al* 2016, Cates and Craig 2019, Ota *et al* 2019, Gundacker *et al* 2020, Ariño-Estrada *et al* 2021, Kratochwil *et al* 2021a, 2021b, Terragni *et al* 2022, Gundacker *et al* 2023, Jens and Vandenberghe 2023, Kratochwil 2023).

In this manuscript, we evaluate the timing performance of the FastIC in combination with the latest generation of analog SiPMs from FBK (NUV-HD-MT technology) coupled to BGO and LSO:Ce:0.2%Ca crystals. Both the intrinsic timing capability using small crystals as well as the performance with long crystals, which are typically used in PET scanners, are investigated. To have a fair evaluation with the state-of-the-art time resolution with minimal impact of electronic noise and time walk effects, comparison measurements with custom high frequency readout electronics of the same detectors were performed.

2. Materials and methods

2.1. Scintillating crystals

Measurements were performed with different crystals summarized in table 2, always wrapped in several layers of Teflon and glued with Cargille Melmount (refractive index $n_c = 1.582$) to the SiPMs. Two distinct crystal materials were evaluated: lutetium oxyorthosilicate doped with cerium and co-doped with 0.2% calcium (LSO:Ce:0.2%Ca) and bismuth germanate (BGO).

2.2. Silicon photomultipliers

Initial test measurements were performed with SiPMs from Hamamatsu photonics (S13360 3050PE), as they have been commercially available for a long time and thus the most common sensor used in literature, and with FBK NUV-HD-MT SiPMs. After confirming the superior timing performance (Gundacker *et al* 2020, Kratochwil *et al* 2021a) of the NUV-HD(-MT) technology, to be valid also for FastIC, in-depth measurements were performed using only the mentioned new MT-technology from FBK. The SiPMs have a pixel pitch of 40 μm with an effective photosensitive area of $3 \times 3 \text{ mm}^2$ and no protective resin. The intrinsic SPTR of the SiPMs was measured to be about 50 ps FWHM after correcting for the electronic noise and contribution of the laser jitter/ reference detector (Gundacker *et al* 2023, Penna *et al* 2023).

2.3. Coincidence time resolution (CTR) setups

Two different CTR setups were used for the evaluation of timing performance. The first one is based on high frequency (HF) readout electronics (Cates *et al* 2018, Gundacker *et al* 2019) and a LeCroy DDA735Zi (3.5 GHz, 20 Gs s^{-1}) oscilloscope (Gundacker *et al* 2016a). A balun transformer in combination with two radio frequency

Table 1. Summary of ASICs used for TOF measurements. Due to the use of different SiPMs, scintillators and measurement setups, it is not always possible to directly compare the values, thus the table is intended to provide an overview and references to literature.

ASICs	Ch.	Power [mW/ch]	SPTR				CTR				
			Value [ps]	FWHM [ps]		Laser [nm]	Value [ps]	FWHM [ps]		SiPM	
				Type	Size ^a			Crystal [mm ³]	Type		Size ^a
TOFPET2 ^c	64	8	195	HPK S14160	3 × 3, 50	N/A	134	LYSO:Ce:Mg, 2 × 2 × 3	HPK S14160	3 × 3, 50	
NINO ^d	8	27	160	HPK S13360	3 × 3, 50	420	73	LSO:Ce:Ca, 2 × 2 × 3	FBK NUV-HD	4 × 4, 25	
Petiroc 2A ^e	32	6	200	HPK S13360	3 × 3, 50	N/A	127	LSO:Ce:Ca, 2 × 2 × 3	FBK NUV-HD	4 × 4	
Triroc 1A ^f	64	10	N/A				433	LYSO, 3 × 3 × 10	ADVANSID NUV	N/A	
Liroc ^g	64	3.3	169	HPK S13361	2 × 2, 50	N/A	N/A				
Radiroc ^h	64	N/A	73	NUV-HD-LF M3	1 × 1, N/A	^b	83	LYSO, 2 × 2 × 3	NUV-HD-MT	N/A	
STiC ⁱ	64	25	158	HPK 13 360	1.3 × 1.3, 50	460	214	LYSO:Ce, 3.1 × 3.1 × 15	HPK S12643	3 × 3, 50	
DIET ^j	64	5	N/A				334	LYSO, 2 × 2 × 11	SensLFJ	3 × 3, 35	
ToT-ASIC2 ^k	64	2.9	N/A				215	GFAG (8 × 8), 2.5 × 2.5 × 5	HPK S13361 (8 × 8)	3 × 3, 50	
HRFle × ToT ^l	16	3.5	167	HPK S13360	3 × 3, 50	405	118	LSO:Ce:Ca0.4%, 2 × 2 × 5	HPK S13360	3 × 3, 50	
FastIC ^m	8	12	140	HPK 13 360	3 × 3, 50	635	105	LSO:Ce:Ca0.2%, 2 × 2 × 5	HPK S13360	3 × 3, 50	

^a Area [mm²], pixel pitch [μ m].

^b Black painted PbF₂ crystal, see (Kratochwil *et al* 2021b) for the method.

^c (Bugalho *et al* 2018, 2019, Nadig *et al* 2022).

^d (Anghinolfi *et al* 2004, Gundacker *et al* 2016a, Nemallapudi *et al* 2016, Gundacker *et al* 2019).

^e (Ahmad *et al* 2018).

^f (Ahmad *et al* 2015, 2016, Belcari *et al* 2019).

^g (Liroc, , Saleem *et al* 2023).

^h (Contino *et al* 2020, Saleem *et al* 2023).

ⁱ (Chen *et al* 2014, Harion *et al* 2014, Munwes *et al* 2015), SPTR measurement with a focused laser beam with spot size of a few μ m.

^j (Chen *et al* 2018).

^k (Orita *et al* 2023).

^l (Sarasola *et al* 2017, David Sánchez *et al* 2022).

^m (Gomez *et al* 2021, 2022).

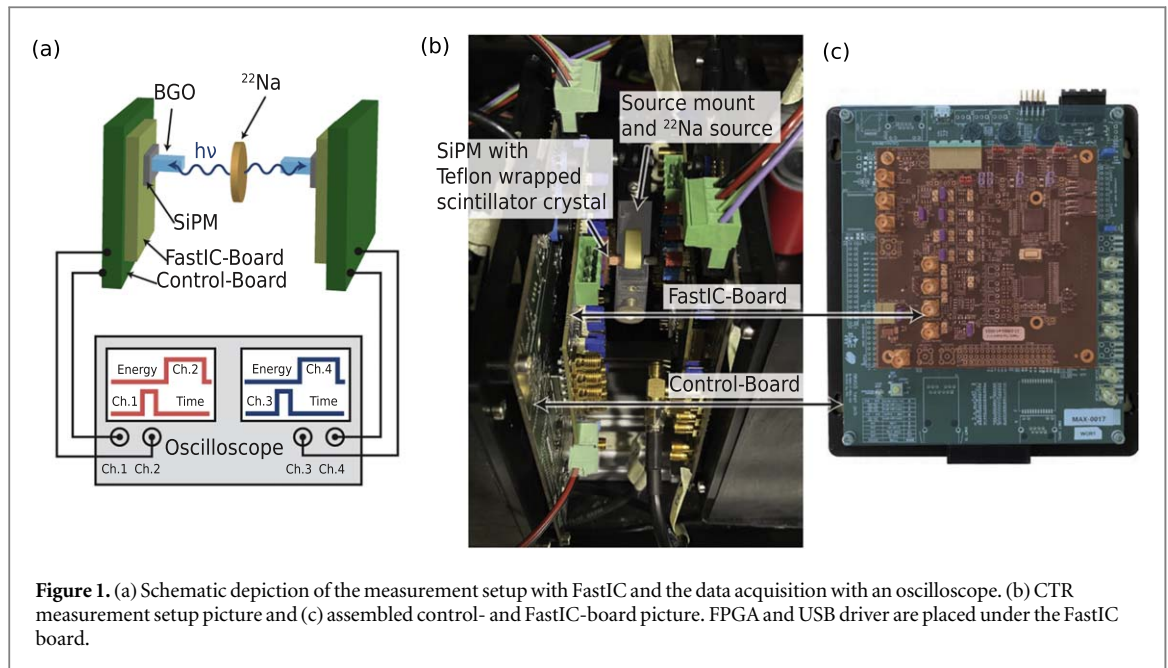


Table 2. Overview of scintillator crystals used in this work.

Material	Manufacturer	Peak emission [nm]	Size [mm ³]	Effective decay time ^a [ns]	Intrinsic light yield ^a [ph keV ⁻¹]
LSO:Ce:0.2%Ca	Agile	420	2x2x3 2x2x20	31.5	39.2
BGO	EPIC	480	2x2x3 2x2x20	234.3	10.7

^a Gundacker *et al* (2020).

amplifiers was used to generate a fast analog time signal used for leading edge discrimination, while an analog operational amplifier (AD8000) was employed to monitor the number of detected emitted photons (energy signal). A comprehensive discussion of the setup and implementation of the custom readout electronics is given in Gundacker *et al* (2019).

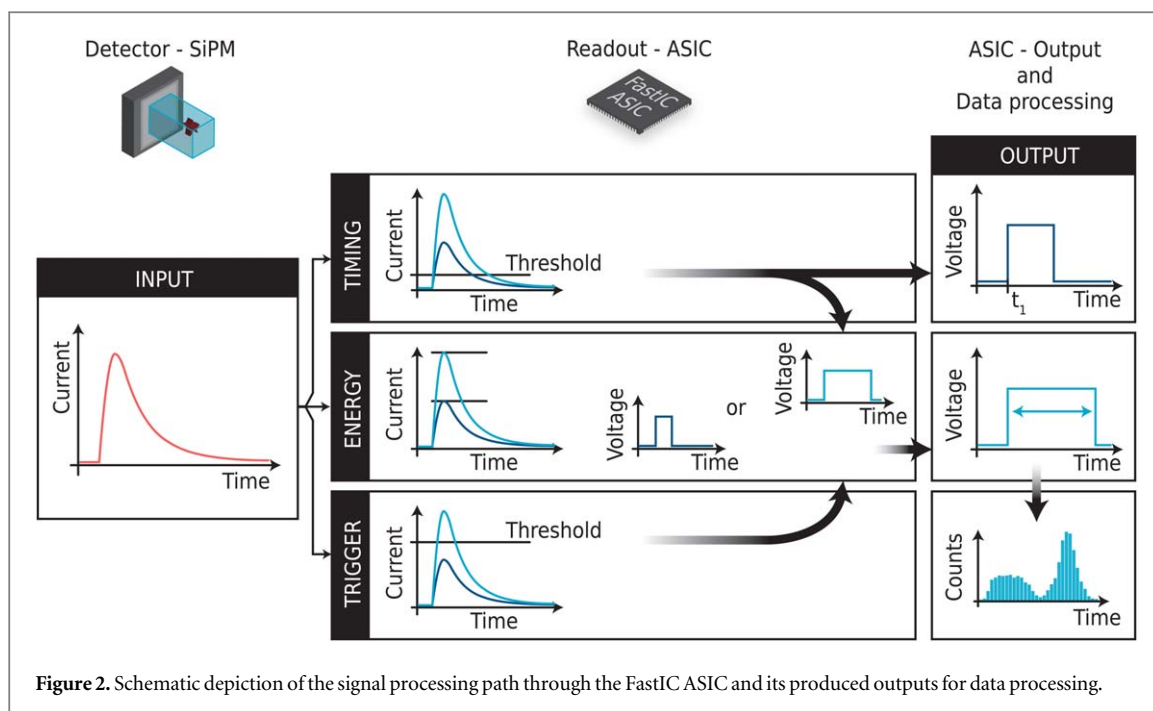
For the second setup, two FastIC-evaluation demonstrator boards (ICC-UB 2023) were used, consisting of two stacked printed circuit boards, namely the FastIC board and a control board shown in figures 1 (a)–(c).

The FastIC board features sockets for testing individual SiPMs and SiPM arrays, along with a dedicated high-voltage power supply connection. Additionally, it offers various output access options for the ASIC (Gomez *et al* 2021). The control board facilitates the configuration of the FastIC ASIC via a computer, using a FPGA (Speed Grade 7 Intel MAX 10) for slow control and a USB driver for communication. The produced output signals were captured using a LeCroy WaveRunner 104MXi-a oscilloscope (1 GHz, 10 Gs s⁻¹). The oscilloscope is set to trigger based on the simultaneous energy signals, and data regarding energy and time are directly measured in the oscilloscope from each acquired waveform.

2.4. FastIC signal processing

The input signal generated by the SiPM following a gamma-ray interaction in the crystal is processed by the FastIC front-end electronics. It triplicates the current pulse to three signal processing paths with different internal gains with the task of individually providing information on the timing, energy and triggering as illustrated in figure 2.

The timing path always creates an output pulse after the signal crosses a certain time threshold set by a comparator. The timing information is encoded on the rising edge. The energy processing path produces a linear energy output pulse with the energy information encoded in the pulse width. The FastIC offers two configurable options for energy output signal generation. The first option involves generating the signal when it exceeds the set timing threshold. The second option generates the signal only when it reaches a predetermined threshold in the triggering path. As illustrated in figure 2, this feature provides the flexibility to choose the most appropriate method for a certain application. In this work, the FastIC was configured with the second option. The gain on the energy path can be adjusted to count either individual photons or measure thousands of scintillating photons. In



a similar manner, the timing and trigger threshold can be adjusted with the aim of providing a low leading edge threshold (typically at the level of 10% to 200% of a single SPAD signal amplitude) and a flexible trigger threshold aiming to discard dark count events and events with low energy deposition.

Energy (based on the linear measurement of the signal amplitude) and timing signal are combined into one signal, with the first pulse providing the timing information and the second pulse containing the energy information. However, in this study, we disabled the timing pulse and routed it via fast-OR signal to a different output channel.

Figure 3 illustrates the two potential setups. In option 1, depicted in (a), the energy and timing signals are merged into a single signal, where the initial pulse conveys timing details through the rising edge, and the subsequent pulse encodes energy information within the pulse duration. For this study, option 2 was employed, as shown in (b), where the timing and energy pulses are distinct and captured using separate channels on an oscilloscope (c).

Although option 2 doubles the number of readout channels, it simplifies the oscilloscope's data acquisition process, allowing individual signal processing. In total 4 channels (2 for timing, 2 for energy) were used.

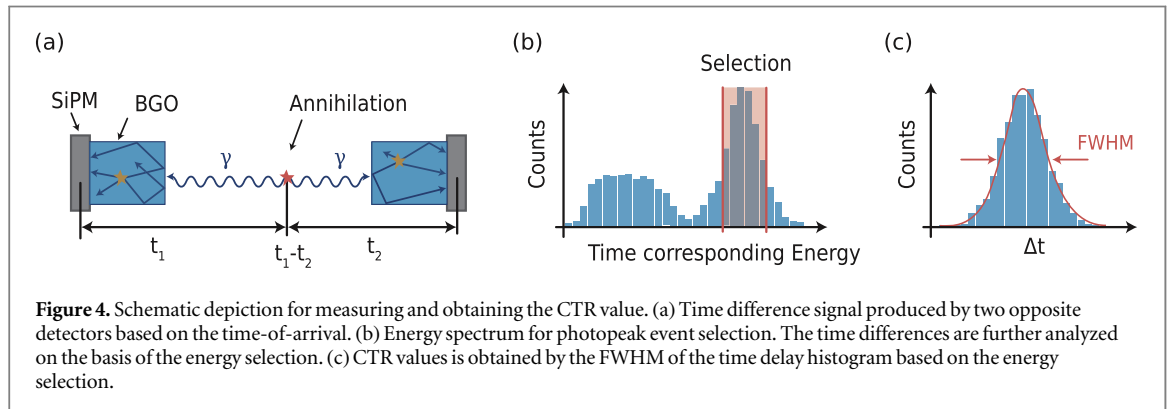
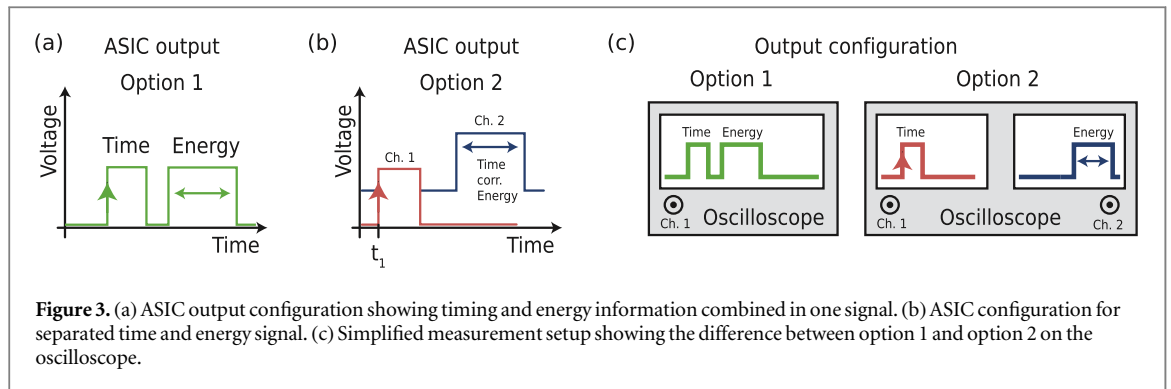
Since the FastIC output signals are binary pulses, the performance of the digitizer is less demanding with respect to fully analog signals as long as the sampling rate is sufficient to capture points on the rising edge.

2.5. Data analysis

At least 10 000 coincidence events were recorded for both setups and each configuration. The CTR was determined by calculating the time difference between the arrival times of signals from opposite-facing sensors, as shown in figure 4(a). The signal integral (HF readout) or signal amplitude (encoded in the width of the pulse) was used for energy discrimination selecting at 511 keV photopeak events as illustrated in figure 4 (b). In particular, a Gaussian fit of the photopeak region is performed, and the center of the Gaussian at 511 keV plus or minus 1.5 times the standard deviation is used to perform the energy cut. With a measured energy resolution of BGO (without SiPM saturation correction) of 20%, this translates to an energy window between 440 keV and 570 keV. For the selected events, the time difference is histogrammed as shown in figure 4 (c) and the CTR value is obtained as the full width at half maximum (FWHM) of the coincidence time delay histogram. For measurements with LSO, the time difference was modeled with a simple Gaussian distribution, while for BGO measurements, a fit consisting of two Gaussian distributions was used (Kratochwil *et al* 2021a) and the FWHM calculated as the difference between the crossing points of half the maximum.

2.6. Photon counting for FastIC threshold configuration

To calibrate the threshold settings for the FastIC, staircase plots were generated by quantifying the number of cells triggered at different threshold levels (in units of LSB) with the FPGA. The photon count data obtained at different SiPM overvoltages and different gains (I_{LSB} dictates the increment between two consecutive thresholds) are presented in figure 5. The I_{LSB} therefore controls the size and number of steps in the threshold sweep. It can



be seen that for high overvoltage only a few stairs are visible and each step ranges over multiple threshold values, while for lower overvoltage the effective DCR is drastically reduced due to a combination of low gain (thus the threshold is at the level of several triggered cells) and low SiPM crosstalk probability (it becomes less likely that a single dark count in a cell triggers multiple cells).

To have sufficient dynamic range, but also fine granularity around the level of a single triggered SPAD, a global I_{LSB} setting of 15 was used for the following measurements.

3. Results

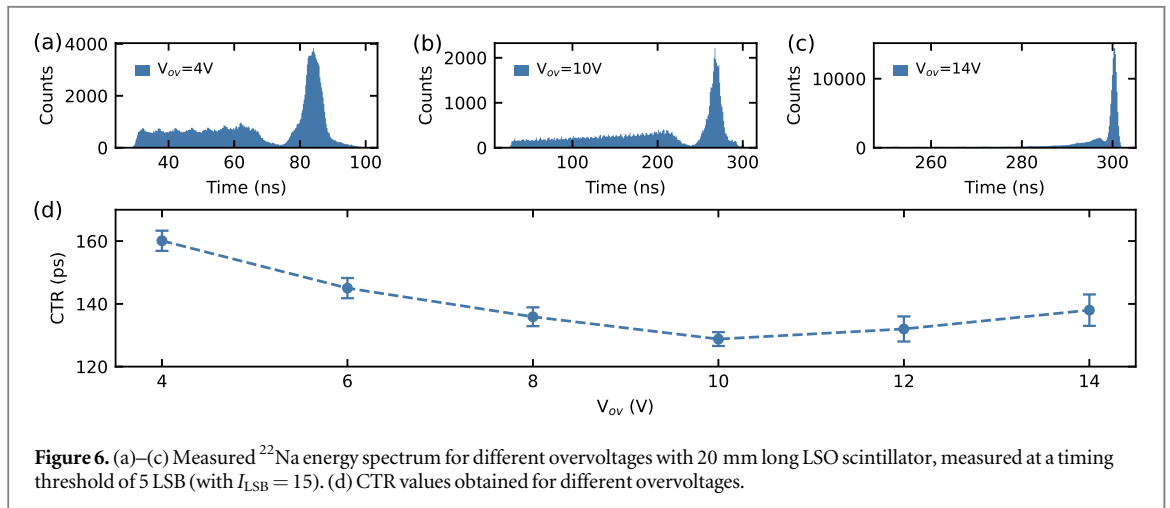
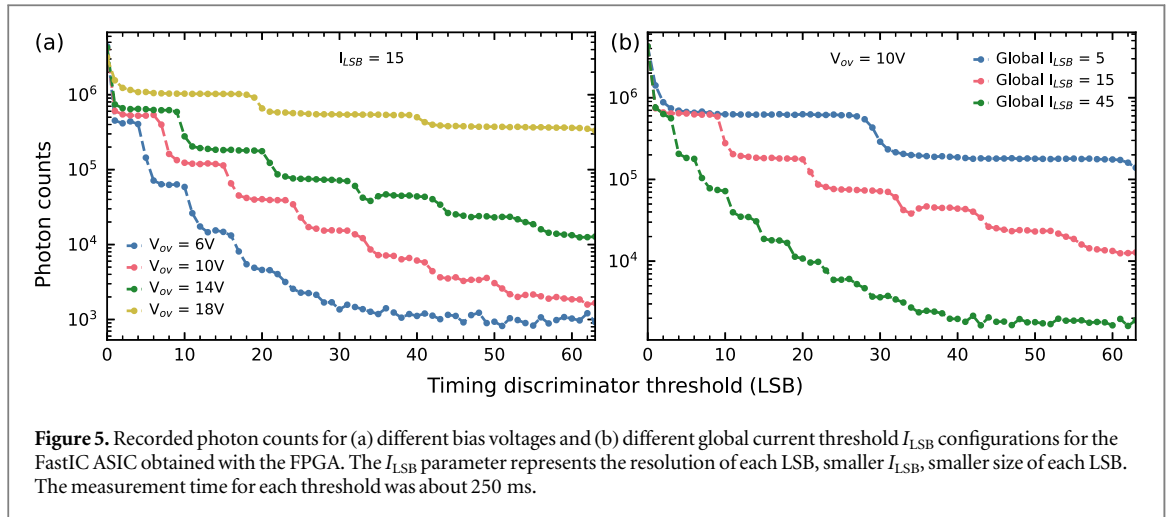
3.1. SiPM overvoltage scan and saturation of the energy signal

One advantage of the new MT-technology is the reduction of internal crosstalk, which allows to bias the SiPMs at higher overvoltage to increase gain, PDE and SPTR (Merzi *et al* 2023). To make use of this improvement, CTR measurements were performed at different SiPM overvoltages with 20 mm long LSO crystals. Figure 6 shows the obtained energy histograms at different SiPM overvoltages (a)–(c) as well as the CTR as function of the overvoltage (d). It can be seen that for high overvoltage the dynamic range of the ASIC reaches its limitation, as the Compton edge and photopeak are no longer well resolvable. Thus, at higher overvoltage also events depositing less energy in the crystal were considered which degrades the measured CTR. The best CTR value of 133 ± 5 ps was achieved at 10 V overvoltage. For these measurements, the timing discriminator threshold was not optimized.

3.2. CTR results for BGO and LSO with the FastIC

For the optimum overvoltage of 10 V, a threshold scan was performed for all tested crystals. Following the performed calibration in figure 5, the amplitude of a single SPAD cell corresponds to about 8 LSB, thus the scan ranges from [0–4] triggered SPADs for BGO and [0–2.5] triggered SPADs for LSO. The top of figure 7 (a)–(c) shows the selected energy selection for 20 mm long BGO crystals and the resulting coincidence time delay distribution, while in the bottom the CTR as function of the discriminator threshold is plotted for (d) BGO and (e) LSO.

The reference measurement of the small BGO crystals coupled to HPK SiPMs is also included, showing that the FBK sensors achieve about 30% better time resolution with respect to the HPK technology. This trend is consistent with published data in Kratochwil *et al* (2021a) using HF readout electronics.



For BGO, operating at very low threshold settings is vital to preserve the good timing response arising from the detection of prompt Cherenkov emission with measured CTR values of 330 ± 8 ps FWHM for small pixels and 490 ± 12 ps FWHM for 20 mm long crystals. Given the bright and fast scintillation response of LSO, there is only a small threshold dependency for LSO (Seifert *et al* 2012), resulting in measured CTR values of 95 ± 3 ps and 129 ± 4 ps FWHM for 3 mm and 20 mm long crystals respectively.

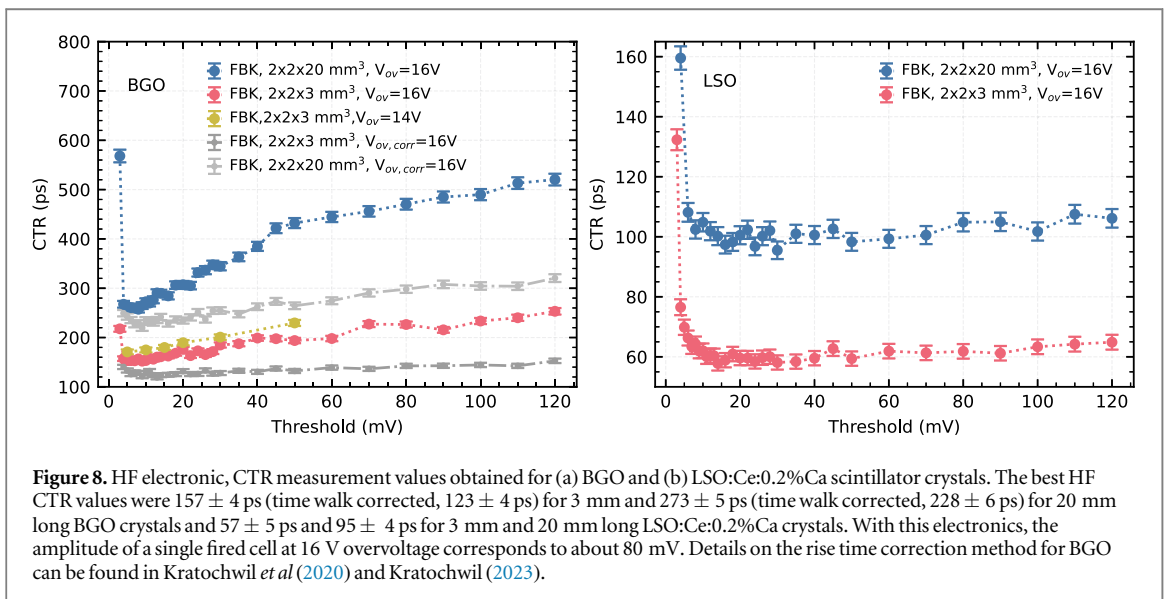
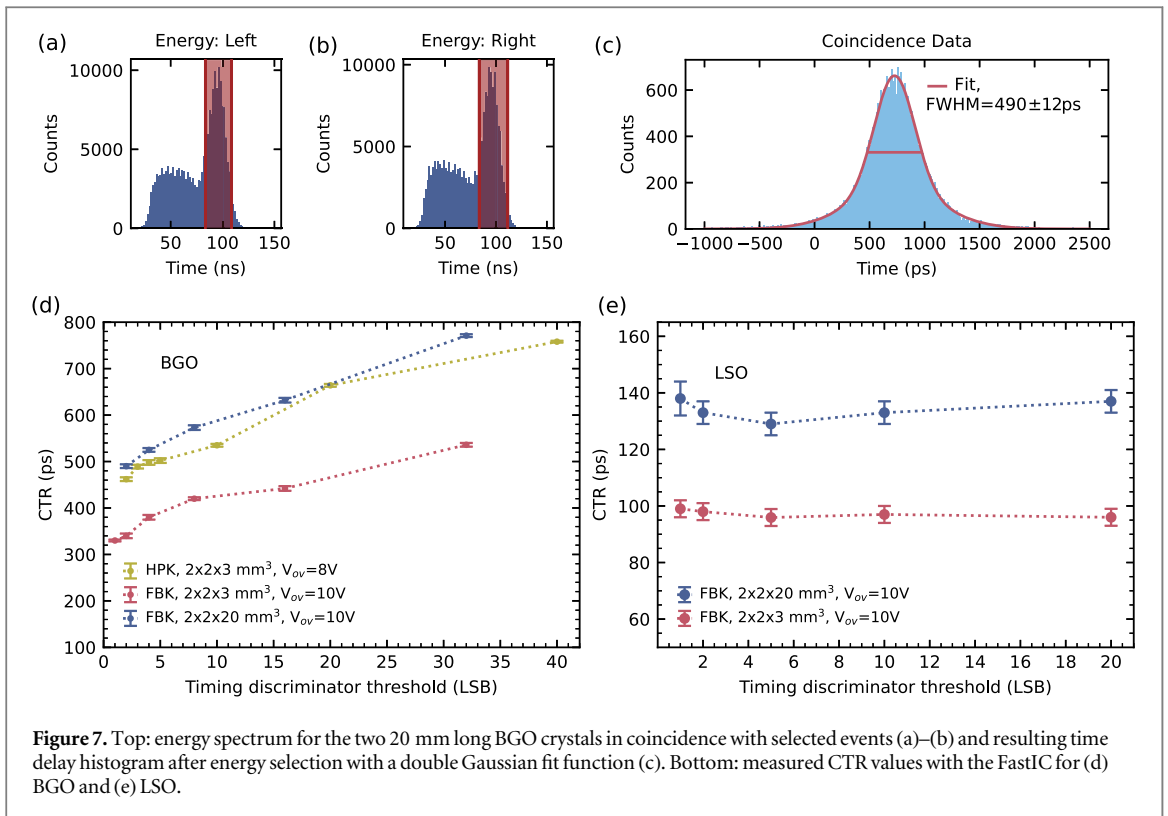
The energy resolution obtained by FastIC at 511 keV is approximately 22% for the 20 mm long crystals and 20% for the 3 mm long crystals without applying any correction for SiPM saturation. The non-linearities of SiPM at large signals should not be significant for BGO due to its low light yield compared to LSO crystals that requires to compensate this non-linearity to compute the energy resolution (David Sánchez *et al* 2022).

3.3. Timing limits with HF readout electronics

The timing performance of the same detectors (crystals glued to SiPMs) was also investigated with high power consuming readout electronics to assess the intrinsic limits. In this case, there was no limitation on maximum overvoltage, meaning that the SiPMs were biased up to 16 V above breakdown voltage. In figure 8 the measured time resolution as function of the leading edge threshold is shown for (a) BGO and (b) LSO.

Particularly for the long BGO crystal, one can observe a strong threshold dependency and the optimum settings are reached for values just above the electronic noise floor.

Although not scalable to a full system, the obtained CTR values for LSO and BGO (upon time walk correction) are consistent with measurements reported in Gundacker *et al* (2020), (2023), Nadig *et al* (2023) with the same SiPM technology.



4. Discussion and outlook

4.1. Comparison of readout electronics for LSO

Comparing the obtained CTR results for the FastIC with HF readout electronics, we notice an offset of about 30 ps for LSO with the ASIC for both crystal geometries. Such an offset is expected due to the following reasons: first, the FastIC input stage might be limited in the bandwidth meaning in combination with the capacitance of the SiPM and additional impedance from the connectors, it reduces the effective bandwidth (Fernández-Tenllado *et al* 2019). This means that the SiPM signal slew rate (dV/dt) is lower, resulting in an additional contribution of electronic noise (Cates *et al* 2018). Due to this electronic noise contribution, the optimal threshold is reached at higher leading edge threshold settings (eg, for 20 mm long LSO at 5 LSB ($\approx 60\%$ of a single SPAD signal amplitude), compared to ≈ 20 mV (25% of a single SPAD signal amplitude) for the FastIC and HF readout, respectively). Although LSO is a bright scintillator with many photons produced in the first few

nanoseconds, having the timestamp at a later time can worsen the statistical contribution of the scintillation response (Seifert *et al* 2012). Due to the interplay between electronic noise contribution (scaling inverse, $\text{CTR} \propto 1/\text{threshold}$) and photo statistics (scaling linear, $\text{CTR} \propto \text{threshold}$ with the leading edge threshold (Gundacker *et al* 2020)), the optimum settings are reached at higher values for the FastIC.

Next, the timestamp for the FastIC measurement is obtained by the in-built timing comparator, which has limited performance. On the contrary with the HF readout measurement, the timing is obtained via leading edge discrimination directly on the high-performance oscilloscope with negligible timing jitter.

Lastly, the FastIC was limited in terms of signal saturation at high overvoltage, thus lower bias voltage had to be applied. Both PDE and measured SPTR improve further by a few percentage when increasing the excess bias voltage above 10 V (Merzi *et al* 2023). Adjusting the overvoltage to 10 V for the HF readout measurement results in a mild CTR degradation from 57 ± 5 to 64 ± 4 ps for the small and from 95 ± 3 to 104 ± 3 ps FWHM for the long LSO crystals.

As mentioned before, the performance of the digitizer/oscilloscope is negligible due to the digital-like output signal of the FastIC. With a measured signal slope (dV/dt) of 1.2 V ns^{-1} and a RMS of the baseline of 3 mV, this translates into a jitter ($\sigma_{\text{digitizer}} = 2.35 \cdot \frac{\text{RMS}}{dV/dt}$) of 6 ps per channel. Correcting for does only change the decimal place, eg. from 95 to 94.6 ps FWHM.

4.2. Comparison of readout electronics for BGO

All the mentioned considerations are also valid for BGO, however the impact is more severe in the case of prompt photons. Given the low amount of detected light, the analog signal slew rate of the SiPM is smaller, hence higher electronic jitter. Placing the leading edge threshold at higher values when the signal is steeper does not help either, because by then we face strong statistical fluctuations based on the number of detected prompt photons (Kratochwil *et al* 2021a). Given those considerations, having a low electronic noise contribution already at very low leading edge thresholds is crucial for low light intensities (Dolenec *et al* 2016, Kratochwil *et al* 2021b). Another aspect, more dominant for Cherenkov photons in BGO, are time-walk effects. For a higher leading edge threshold, time-walk effects have more time to propagate and contribute. This behavior can be well observed for the threshold scan with the HF readout measurement displayed on the left of figure 8, with measured CTR values of 157 ± 4 ps at 10 mV (12% of the single SPAD signal amplitude), 176 ± 4 ps at 20 mV (25% of the single SPAD signal amplitude), and 199 ± 4 ps at 40 mV (50% of the single SPAD signal amplitude).

Also, the limitation in overvoltage contributes, for instance at 12 V overvoltage instead of 16 V, the measured CTR values with HF readout electronics are 172 ± 5 ps FWHM and 296 ± 6 ps for the small and long crystals, respectively, while for 16 V overvoltage the CTR values are 157 ± 4 ps and 273 ± 5 ps.

4.3. Time walk correction

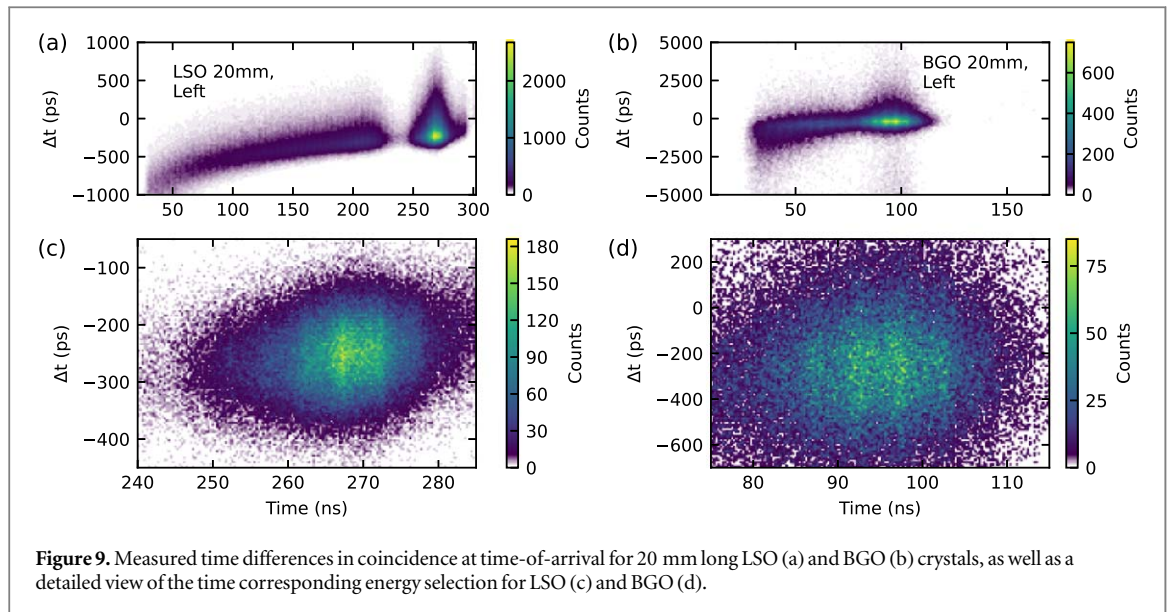
For leading edge discrimination, it is normal to experience some kind of time-walk as signals with a high number of detected photons pass the threshold earlier compared to signals with a lower number. Hereby, the selected energy window is a determining factor: for a narrow energy selection, we can assume that the signal variation is small, and hence little jitter comes from these variations. In addition, the magnitude of time-walk effects depends on the value of the leading edge threshold- as mentioned before placing it at high values means variations of the signal have more time to propagate, enhancing the effect.

To assess the potential contribution with the FastIC measurements coming from time walk, the coincidence time delay is plotted against the signal amplitude (expressed as time due to the nature of the energy measurement) for 20 mm long LSO (left) and 20 mm long BGO (right) crystals in figure 9.

In both cases we observe time walk effects when selecting all the events (top), while after photopeak selection (bottom) there is no clear time-walk visible and therefore no additional room for improvement.

For the special case of Cherenkov radiation in BGO, there is another fluctuation due to the number of detected prompt photons. It was shown in Kratochwil *et al* (2020) that by measuring the signal rise time of the analog amplified signal, these fluctuations can be monitored on an event-to-event basis and corrected with respective time resolution improvements.

Although for the measurement with HF electronics we were able to access the signal rise time and perform such a correction (resulting in a CTR improvement from 157 ± 4 to 123 ± 4 ps) for 3 mm and 273 ± 5 to 228 ± 6 ps) for 20 mm long BGO crystals, in depth discussed in Kratochwil (2023)), for the FastIC measurements we only have one timestamp available, and thus no access to monitor signal variations coming from the detection of prompt photons. One solution—on a single pixel level and solely as proof of concept—might be to utilize the trigger signal to get a second timestamp and from this calculate the signal rise time as the difference between the timestamps generated by the FastIC timing output and the trigger output. However, this requires substantial modifications on the data acquisition and yields a lot of unwanted signals (as the trigger threshold should be set low, in the level of a few triggered SPADs, where we capture many dark count events).



Moreover, the trigger signal has a larger jitter, adding another source of variation that needs to be taken into account in accurately measuring the rise time with two thresholds. Verifying this workaround to validate the applicability of time-walk correction for prompt photons with an ASIC is subject to dedicated future work.

4.4. Impact of the energy window on the timing performance with BGO and the FastIC

Similar to Kratochwil *et al* (2021b), we tested the impact of the energy window on the achievable timing resolution with the 20 mm long BGO crystals. Adjusting the upper energy windows (above the 1.5 standard deviations, about 570 keV) has a negligible effect on the CTR values, whereas modifying the lower energy threshold can impact the CTR. Changing the lower energy threshold from 440 to ≈ 400 keV, ≈ 300 keV and ≈ 150 keV yields CTR values of 490 ps, 500 ps, 540 ps and 600 ps respectively. The timing degradation is mild, mostly because the majority of the events (given the high photofraction in BGO) deposit the full energy in the crystal.

This means, that accepting low energy events on a BGO TOF-PET scanner based on the FastIC would further enhance the good sensitivity with only a mild timing degradation. However, this sensitivity gain comes with a drop in spatial resolution and selecting the optimum configuration will depend on the specific imaging task.

4.5. FastIC+ and considerations toward a system

In this study, an evaluation of the FastIC was performed based on single channels. The aim was to expand the range of performance already studied (Gomez *et al* 2021, Mariscal-Castilla *et al* 2023) and to gain a better understanding of how this ASIC works with the most recent SiPM technology in combination of prompt Cherenkov emission. Although the CTR values are better with HF readout electronics, the obtained results with the FastIC are scalable. Each of the FastIC boards is equipped with two ASICs, thus in total 16 channels (e.g. 4 x 4 SiPM crystal array) can be read out with low power consumption of only 12 mW/channel. The current version does not include a time-to-digital converter (TDC), thus the requirements on the signal processing are high. This major limitation is addressed in the successor chip FastIC+, which will include a TDC with a simulated jitter contribution of only 22 ps FWHM.

We can expect mild timing degradation (Nadig *et al* 2023b) when using 1:1 crystal-SiPM coupling and due to light sharing / enhanced SiPM crosstalk for the full SiPM array. However, already a CTR of 500 ps on a system level constitutes a more than factor 5 gain of effective sensitivity with respect to non-TOF capability assuming a diameter object of about 40 cm (Maurizio 2009).

5. Conclusion

In this study, we have presented the results of our examination of the FastIC readout ASIC with Cherenkov emitting scintillators and one of the most recent SiPM detector developments. The best measured coincidence resolution at 511 keV the FastIC were 330 ps and 490 ps FWHM for small and long BGO crystals. Although the CTR values are substantially better using power-hungry high frequency readout electronics, already these figures show the potential of the FastIC as a readout ASIC for TOF-PET applications utilizing Cherenkov-emitting

scintillators. For state-of-the-art LSO scintillators coupled to FBK NUV-HD MT SiPMs and read out with the FastIC, we demonstrate sub-100 ps for 3 mm long crystals, and even for 20 mm long crystals the timing deterioration is only about 30 ps with respect to the limits with HF-readout electronics.

Further research is necessary to determine whether and to which extent the addressed limitations in terms of electronic noise and time-walk contribution can be overcome. Additionally, a study is required to determine whether an increase in the dynamic range of the ASIC would improve the CTR performance for SiPMs with MT-technology. Although this study focused on the performance evaluation on a single channel level, the reported encouraging results are scalable, and no substantial timing degradation is expected. The findings underscore the potential of the FastIC ASIC in the development of cost-effective TOF-PET scanners with excellent timing characteristics.







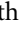


Acknowledgments

Markus Piller and Giulia Terragni received support from the Federal Ministry of Education, Science and Research of Austria (Austrian Doctoral Student Programme at CERN). This work was partly performed in the framework of the Crystal Clear Collaboration and received support from CERN budget from knowledge transfer to medical applications.

Data availability statement

All data that support the findings of this study are included within the article (and any supplementary information files).

ORCID iDs

Markus Piller  <https://orcid.org/0000-0002-1408-2962>
Giulia Terragni  <https://orcid.org/0000-0002-1030-0758>
Etiennette Auffray  <https://orcid.org/0000-0001-8540-1097>
David Gascon  <https://orcid.org/0000-0001-9607-6154>
Alberto Gola  <https://orcid.org/0000-0002-5278-5044>
Stefano Merzi  <https://orcid.org/0000-0002-0512-2491>
Alicja Michalowska-Forsyth  <https://orcid.org/0000-0003-2419-1406>
Sergio Gómez  <https://orcid.org/0000-0002-3064-9834>
Nicolaus Kratochwil  <https://orcid.org/0000-0001-5297-1878>

References

- Ahmad S, de la Taille C, Fleury J, Seguin-Moreau N, Raux L, Callier S, Martin-Chassard G, Dulucq F and Thienpont D 2016 Triroc, a versatile 64-channel SiPM readout ASIC for time-of-flight PET 2016 *IEEE Nuclear Science Symp., Medical Imaging Conf. and Room-Temperature Semiconductor Detector Workshop (NSS/MIC/RTSD)* 1–5
- Ahmad S, Fleury J, Cizel J-B, de la Taille C, Seguin-Moreau N, Gundacker S and Auffray-Hillemanns E 2018 Petiroc2a: characterization and experimental results 2018 *IEEE Nuclear Science Symp. and Medical Imaging Conf. Proc. (NSS/MIC)* pp 1–4
- Ahmad S, Fleury J, de la Taille C, Seguin-Moreau N, Dulucq F, Martin-Chassard G, Callier S, Thienpont D and Raux L 2015 Triroc: a multi-channel SiPM read-out ASIC for PET/PET-TOF application *IEEE Trans. Nucl. Sci.* **62** 664–8
- Anghinolfi F, Jarron P, Krummenacher F, Usenko E and Williams M C S 2004 Nino: an ultrafast low-power front-end amplifier discriminator for the time-of-flight detector in the alice experiment *IEEE Trans. Nucl. Sci.* **51** 1974–8
- Ariño-Estrada G, Roncali E, Selfridge A R, Du J, Shah K S and Cherry S R 2021 Study of Čerenkov light emission in the semiconductors t1br and t1cl for TOF-PET *IEEE Trans. Radiat. Plasma Med. Sci.* **5** 630–7
- Belcari N, Bisogni M G, Camarlinghi N, Carra P, Cerello P, Morrocchi M, Patera A, Sportelli G and Guerra A D 2019 Design and detector performance of the PET component of the TRIMAGE PET/MR/EEG Scanner *IEEE Trans. Radiat. Plasma Med. Sci.* **3** 292–301
- Bugalho R et al 2018 Experimental results with TOFPET2 ASIC for time-of-flight applications *Nucl. Instrum. Methods Phys. Res. A* **912** 195–8
- Bugalho R et al 2019 Experimental characterization of the TOFPET2 ASIC *J. Instrum.* **14** P03029
- Cates J W and Choong W-S 2022 Low power implementation of high frequency SiPM readout for Cherenkov and scintillation detectors in TOF-PET *Phys. Med. Biol.* **67** 195009
- Cates J W and Craig C S 2019 Electronics method to advance the coincidence time resolution with bismuth germanate *Phys. Med. Biol.* **64** 175016
- Cates J W, Gundacker S, Auffray E, Lecoq P and Levin C S 2018 Improved single photon time resolution for analog SiPMs with front end readout that reduces influence of electronic noise *Phys. Med. Biol.* **63** 185022
- Cates J W, Steele J, Balajithy J, Negut V, Hausladen P, Ziock K and Brubaker E 2022 Front-end design for SiPM-based monolithic neutron double scatter imagers *Sensors* **22**
- Chen H et al 2014 A dedicated readout ASIC for time-of-flight positron emission tomography using silicon photomultiplier (SiPM) 2014 *IEEE Nuclear Science Symp. and Medical Imaging Conf. (NSS/MIC)* pp 1–5

- Chen Y, Deng Z and Liu Y 2018 DIET: a multi-channel SiPM readout ASIC for TOF-PET with individual energy and timing digitizer *J. Instrum.* **13** P07023–07023
- Contino G et al 2020 An ASIC front-end for fluorescence and Cherenkov light detection with sipm for space and ground applications *Nucl. Instrum. Methods Phys. Res. A* **980** 164510
- David Sánchez S et al 2022 Hrflexot: a high dynamic range ASIC for time-of-flight positron emission tomography *IEEE Trans. Radiat. Plasma Med. Sci.* **6** 51–67
- Dolenec R, Korpar S, Križan P and Pestotnik R 2016 Sipm timing at low light intensities 2016 *IEEE Nuclear Science Symp., Medical Imaging Conf. and Room-Temperature Semiconductor Detector Workshop (NSS/MIC/RTSD)* pp 1–5
- Fernández-Tenllado J M, Ballabriga R, Campbell M, Gascón D, Gómez S and Mauricio J 2019 Optimal design of single-photon sensor front-end electronics for fast-timing applications 2019 *IEEE Nuclear Science Symp. and Medical Imaging Conf. (NSS/MIC)* pp 1–5
- Gola A, Acerbi F, Capasso M, Marcante M, Mazzi A, Paternoster G, Piemonte C, Regazzoni V and Zorzi N 2019 NUV-sensitive silicon photomultiplier technologies developed at Fondazione Bruno Kessler *Sensors* **19**
- Gomez S et al 2021 FastIC: a highly configurable ASIC for fast timing applications 2021 *IEEE Nuclear Science Symp. and Medical Imaging Conf. (NSS/MIC)* 00 1–4
- Gomez S et al 2022 FastIC: a fast integrated circuit for the readout of high performance detectors *J. Instrum.* **17** C05027
- Gonzalez-Montoro A, Pourashraf S, Lee M S, Cates J W and Levin C S 2023 Design considerations for pet detectors with 100 picoseconds coincidence time resolution *Nucl. Instrum. Methods Phys. Res. A* **1045** 167579
- Gundacker S, Acerbi F, Auffray E, Ferri A, Gola A, Nemallapudi M V, Paternoster G, Piemonte C and Lecoq P 2016a State of the art timing in TOF-PET detectors with LuAG, GAGG and L(Y)SO scintillators of various sizes coupled to FBK-SiPMs *J. Instrum.* **11** P08008
- Gundacker S, Auffray E, Pauwels K and Lecoq P 2016b Measurement of intrinsic rise times for various L(Y)SO and LuAG scintillators with a general study of prompt photons to achieve 10 ps in TOF-PET *Phys. Med. Biol.* **61** 2802
- Gundacker S, Borghi G, Cherry S R, Gola A, Lee D, Merzi S, Penna M and Kwon S I 2023 On timing-optimized SiPMs for Cherenkov detection to boost low cost time-of-flight PET *Phys. Med. Biol.* **68** 165016
- Gundacker S and Heering A 2020 The silicon photomultiplier: fundamentals and applications of a modern solid-state photon detector *Phys. Med. Biol.* **65** 17TR01
- Gundacker S, Turtos R M, Auffray E, Paganoni M and Lecoq P 2019 High-frequency SiPM readout advances measured coincidence time resolution limits in TOF-PET *Phys. Med. Biol.* **64** 055012
- Gundacker S, Turtos R M, Kratochwil N, Pots R H, Paganoni M, Lecoq P and Auffray E 2020 Experimental time resolution limits of modern SiPMs and TOF-PET detectors exploring different scintillators and Cherenkov emission *Phys. Med. Biol.* **65** 025001
- Harion T, Briggel K, Chen H, Fischer P, Gil A, Kiworra V, Ritzert M, Schultz-Coulon H C, Shen W and Stankova V 2014 STiC—a mixed mode silicon photomultiplier readout ASIC for time-of-flight applications *J. Instrum.* **9** C02003–02003
- ICC-UB 2023 FASTIC documentation and datasheet. Available from: https://icc-ub.gitlab.io/instrumentation/clues/fastic_doc/index.html
- Jens M and Vandenberghe S 2023 Effect of detector geometry and surface finish on cerenkov based time estimation in monolithic BGO detectors *Phys. Med. Biol.* **68** 025009
- Krake M, Nadig V, Schulz V and Gundacker S 2022 Power-efficient high-frequency readout concepts of sipms for TOF-PET and HEP *Nucl. Instrum. Methods Phys. Res. A* **1039** 167032
- Kratochwil N 2023 Studies on time resolution for TOF-PET imaging utilizing Cherenkov emission *PhD Thesis* University of Vienna, Austria <https://ubdata.univie.ac.at/AC17016986>
- Kratochwil N, Auffray E and Gundacker S 2021a Exploring Cherenkov emission of BGO for TOF-PET *IEEE Trans. Radiat. Plasma Med. Sci.* **5** 619–29
- Kratochwil N, Gundacker S and Auffray E 2021b A roadmap for sole Cherenkov radiators with sipms in TOF-PET *Phys. Med. Biol.* **66** 195001
- Kratochwil N, Gundacker S, Lecoq P and Auffray E 2020 Pushing Cherenkov PET with BGO via coincidence time resolution classification and correction *Phys. Med. Biol.* **65** 115004
- Kwon S I, Gola A, Ferri A, Piemonte C and Cherry S R 2016 Bismuth germanate coupled to near ultraviolet silicon photomultipliers for time-of-flight pet *Phys. Med. Biol.* **61** L38
- Lecoq P, Gonzalez A J, Auffray E, Konstantinou G, Nuyts J, Prior J O, Turtos R M and Varela J 2023 Fast timing in medical imaging *IEEE Trans. Radiat. Plasma Med. Sci.* **7** 429–52
- Lee D, Seo M, Cherry S R and Kwon S I 2023 Enhancing performance and resource usage of a multi-channel fpga digitizer for BGO-based time-of-flight (ToF) PET 2023 *IEEE Nuclear Science Symp., Medical Imaging Conf. and Int. Symp. on Room-Temperature Semiconductor Detectors (NSS MIC RTSD)* pp 1–1
- Mariscal-Castilla A et al 2023 Toward sub-100 ps TOF-PET systems employing the fastic ASIC with analog SiPMs *Under Preparation for Submission in IEEE TRPMS*
- Maurizio C 2009 State of the art and challenges of time-of-flight pet *Phys. Med.* **25** 1–11
- Merzi S, Brunner S E, Gola A, Inglese A, Mazzi A, Paternoster G, Penna M, Piemonte C and Ruzzarin M 2023 NUV-HD SiPMs with metal-filled trenches *J. Instrum.* **18** P05040
- Munwes Y, Briggel K, Chen H, Harion T, Schultz-Coulon H-C, Shen W and Stankova V 2015 Single photon time resolution with silicon photomultipliers using the STiC readout chip 2015 *IEEE Nuclear Science Symp. and Medical Imaging Conf. (NSS/MIC)* pp 1–4
- Nadig V, Herweg K, Chou M M C, Lin J W C, Chin E, Li C-A, Schulz V and Gundacker S 2023a Timing advances of commercial divalent-ion co-doped lyso:ce and sipms in sub-100 ps time-of-flight positron emission tomography *Phys. Med. Biol.* **68** 075002
- Nadig V, Hornisch M, Oehm J, Herweg K, Schulz V and Gundacker S 2023b 16-channel SiPM high-frequency readout with time-over-threshold discrimination for ultrafast time-of-flight applications *EJNMMI Physics* **10** 76
- Nadig V, Yusopova M, Radermacher H, Schug D, Weissler B, Schulz V and Gundacker S 2022 A comprehensive study on the timing limits of the TOPPET2 ASIC and on approaches for improvements *IEEE Trans. Radiat. Plasma Med. Sci.* **6** 893–903
- Nemallapudi M V, Gundacker S, Lecoq P and Auffray E 2016 Single photon time resolution of state of the art SiPMs *J. Instrum.* **11** P10016
- Orita T, Uenomachi M, Shimazoe K and Ikeda H 2023 Time and energy resolving time-over-threshold ASIC for MPPC module in TOF-PET system (ToT-ASIC2) *J. Instrum.* **18** P09033
- Ota R, Nakajima K, Ogawa I, Tamagawa Y, Shimoi H, Suyama M and Hasegawa T 2019 Coincidence time resolution of 30 ps FWHM using a pair of Cherenkov-radiator-integrated MCP-PMTs *Phys. Med. Biol.* **64** 07LT01
- Penna M, Acerbi F, Ficorella A, Gola A, Merzi S, Moretti E, Ruzzarin M, Villareal O A M and Zorzi N 2023 Timing performance of FBK SiPM NUV-HD-MT technology using LySO:ce:ca crystal 2023 *IEEE Nuclear Science Symp., Medical Imaging Conf. and Int. Symp. on Room-Temperature Semiconductor Detectors (NSS MIC RTSD)* pp 1–1

- Pourashraf S, Gonzalez-Montoro A, Innes D, Cates J W and Levin C S 2022 Electronic readout for a 100 ps CTR PET detector with 24:1 multiplexing ratio of timing channels *2022 IEEE Nuclear Science Symp. and Medical Imaging Conf. (NSS/MIC)* 1–3
- Saleem T, Ahmad S, Cizel J-B, De La Taille C, Morenas M, Nadig V, Perez F, Schulz V, Gundacker S and Fleury J 2023 Study experimental time resolution limits of recent ASICs at Weeroc with different SiPMs and scintillators *J. Instrum.* **18** P10005
- Sarasola I, Nemallapudi M V, Gundacker S, Sánchez D, Gascón D, Rato P, Marín J and Auffray E 2017 A comparative study of the time performance between NINO and FlexToT ASICs *J. Instrum.* **12** P04016
- Seifert S, Dam H T v and Schaart D R 2012 The lower bound on the timing resolution of scintillation detectors *Phys. Med. Biol.* **57** 1797
- Terragni G, Pizzichemi M, Roncali E, Cherry S R, Glodo J, Shah K, Ariño-Estrada G, Auffray E, Ghezzi A and Kratochwil N 2022 Time resolution studies of thallium based Cherenkov semiconductors *Front. Phys.* **10**
- Weeroc. Liroc, SiPM-based LIDAR Read-Out Chip. Available from: <https://www.weeroc.com/products/sipm-read-out/liroc>